Recent advances in thermoelectric nanocomposites

Citation: Liu, Weishu; Yan, Xiao; Chen, Gang and Ren, Zhifeng. "Recent Advances in Thermoelectric Nanocomposites." Nano Energy 1, 1 (January 2012): 42–56 © 2011 Elsevier Ltd

As Published: http://dx.doi.org/10.1016/j.nanoen.2011.10.001

Publisher: Elsevier

Persistent URL: http://hdl.handle.net/1721.1/110472

Version: Author's final manuscript: final author's manuscript post peer review, without publisher's formatting or copy editing

Recent advances in thermoelectric nanocomposites

Weishu Liu[1], Xiao Yan[1], Gang Chen[2*], and Zhifeng Ren[1*]

[1]Department of Physics, Boston College, Chestnut Hill, Massachusetts 02467

[2]Department of Mechanical Engineering, Massachusetts Institute of Technology, Cambridge, Massachusetts 02139

Abstract

This paper reviews the recent advances in thermoelectric nanocomposite with a special attention on the fundamental tradeoffs dictating the ZT value. A significantly reduction in lattice thermal conductivity has been seen in various material systems with a slight sacrifice of carrier mobility. A new concept of ordered nanocomposite is proposed. It will be a fruitful direction if one could reconstruct the transport channel of electrons current nanocomposite while keeping low lattice thermal conductivity at the same time.

*To whom correspondence should be addressed: gchen2@mit.edu, renzh@bc.edu

1. Instruction

Recent years have witnessed remarkable growing interests in thermoelectric nanocomposite for energy conversion application. One factor driving the current interest in nanocomposite thermoelectric study is the need for safe, cleaning, and sustainable energy source. The crisis at the crippled Fukushima Daiichi nuclear plant due to an earthquake evoked a worldwide re-draft of national future energy strategy. In March 2011, the German government stated that all reactors operational before 1980 in Germany would be taken offline [1]. Solar energy will be the most possible alternative to fill the gap left by the nuclear energy. The amount of radiation energy from sun to earth is gigantic, around 3×10^{24} J/year, which is about 10^4 times more than what humankind consumes currently. In other words, converting the energy received by only 0.1% of the earth's surface with an efficiency of 10% would be enough to satisfy our current needs [2]. However, how to make a reliable and cheap system to convert the solar energy into electric power is still very challenging. The thermoelectric technique has been employed in the Radiative Thermoelectric Generator (RTG) for satellite, deep space exploration missions, such as SNAP-19 for Pioneer 10 mission, which has been working for nearly 40 years [3]. Now, thermoelectrics provides an alternative route to convert the solar energy into electrical power, besides the technology of photovoltaic and thermionic energy conversion. The work principle of thermoelectric module is similar to a heat engine, which employs electrons and holes as the energy carriers. The efficiency of thermoelectrics is governed by the Carnot efficiency and material figure of merit ZT as the following [4],

$$\varphi_{te} = \frac{T_h - T_c}{T_h}\left(\frac{\sqrt{1+Z\overline{T}}-1}{\sqrt{1+Z\overline{T}}+\frac{T_c}{T_h}} \right) \tag{1}$$

where T_h and T_c are the temperatures of the hot and cold end, respectively, $\overline{T}$ is the average temperature between T_h and T_c.

Figure 1 plots the thermoelectric conversion efficiency φ_{te} of single-leg state-of-the-art nanocomposites as a function of temperature difference T_h with an assumption of T_c = 300 K. It is shown that most materials has a thermoelectric conversion efficiency, φ_{te}, ranged from

8%~16.4% [5]-[20] . There remains still large room for future improvement in φ_{te}, since higher ZT value will make the φ_{te} closer to the Carnot efficiency. If only conservative value 70% is used for the opto-thermal conversion efficiency φ_{ot}, the efficiency of solid state solar thermoelectric conversion is 5.6-11.5%. This value competes with the state-of-the-art dye sensitized solar cell (10-11%) [21]. Recently, Kraemer et al. reported that a flat-panel solar thermoelectric generator (STEG) achieved a system efficiency φ_{sys} of 4.6-5.2% ($\varphi_{sys}= \varphi_{ot}\times \varphi_{te}$, φ_{te}=7.4%; φ_{ot}=70-80%) with a temperature difference of 180 ^{o}C (T_c=20 ^{o}C, T_h=200 ^{o}C) [22]. This efficiency is 7-8 times higher than the previously reported best value for a flat-panel STEG. The improvement benefited from the use of high performance nanostructured Bi_2Te_3-based thermoelectric materials and spectrally-selective solar absorber. This work opens up a new cost-effective approach to convert the solar energy into electrical power. STEG is not likely to replace the conventional Stirling or Rankine cycle steam engines in the near future [23]. However, a roof-top STEG has the advantage to help the community members, who cannot afford the cost of power plant and electricity grid in poor country, to improve their life. The combination between flat-panel STEG and water cycle system shows high potential to substitute for the conventional solar water heater, and enables a wide application. Besides the solar energy, the huge amount of waste heat generated from automotives, industry operations, and mankind activities is another energy source for the application of thermoelectric generator. In USA, 191 million vehicles dissipated 66% of energy from gasoline as waste heat, amounting to 36 TWh of waste heat generated from industry operation per year [24].

The efficiency of thermoelectric energy conversion, φ_{te}, is largely determined by the materials figure of merit *ZT* [4], which is defined as $ZT=S^2\sigma T/(\kappa_{lat}+\kappa_{carr}+\kappa_{bipolar})$, where *S*, σ, *T*, κ_{lat}, κ_{carr}, and $\kappa_{bipolar}$ are the Seebeck coefficient, electrical conductivity, temperature, and lattice, electronic and bipolar part of thermal conductivity, respectively. Intuitively, good thermoelectric materials should possess high S to have high voltage output, high σ to reduce Joule heat loss, and low κ to maintain large temperature difference. The normal ways to optimize a material are to increase power factor $S^2\sigma$ by optimizing the carrier concentration n, and to reduce the lattice thermal conductivity κ_{lat} by introducing scatter centers to the phonons. However, the interconnection among these parameters through the more fundamental physical parameters, such as scattering factor *r*, carrier effective mass m^*, and carrier mobility μ, makes the improvement of *ZT* value beyond the benchmark *ZT*=1 difficult for a long time. The

nanocomposite with wider-scale special structure from nano to macro partially breaks the interconnection and shifts the benchmark.

Owing to the wide scope of thermoelectric materials research, which covers theoretical investigation, material design and device assembling with a material form from bulk to low dimension structures, this review only focuses on the basic principle for the challenge behind the *ZT* benchmark value, the recent advances of thermoelectric nanocomposite for potential solid state solar thermoelectric conversion, and the future direction for next generation thermoelectric materials. Interested readers are encouraged to refer to some outstanding review articles, including articles about fundamental phenomena of physics terms contributing to the *ZT* value by Minnich *et al*. [25], by Pichanusakorn *et. al*. [26], and by Shakouri [23], articles about nanostructures modifying the electron and phonon transport by Medlin *et al*. [27], by Lan *et al*. [28], by Li *et al*. [29], by Vineis *et al*. [30], and by Wan *et al*. [31] and articles about special materials such as Clathrates by Kleinke [32], Zintls by Toberer *et al*. [33], PbTe by Kanatzdis [34], Oxides [35], and others [36][37].

2. The challenge behind the benchmark ZT

ZT=1 have been a benchmark for many materials over 30 years since 1960s. The challenge behind the benchmark ZT value is the strong interconnections between 1) S and n, 2) m^* and μ, 3) μ and κ_{lat}, 4) Wiedemann-Franz law, and 5) bipolar effect. The decoupling of relationships among these physical items would give us a chance to push the ZT value beyond the benchmark.

***S* and *n*.** In the kinetic definition, S represents the energy difference between the average energy of mobile carrier and the Fermi energy [26]. An increase in n would cause a simultaneous increase in Fermi energy as well as average energy. However, the Fermi energy will increase much faster than the average energy as n is increased, and therefore lead to a decrease in *S*. Consequently, there is a limit to the S^2n for a material system with a given m^*. The key point to remove the limit for S^2n is by increasing the density of states, i.e. to increases m^*, by introducing resonant states [38], moving the band close to the band edge[39], and by quantum confinement to narrow the DOS [40][41], and by modifying local DOS through introducing nanoinclusions [42]

[43]. In other words, the Seebeck coefficient could be increased by introducing some selective scattering mechanism to filter the low energy carrier and reduce their contribution to Seebeck coefficient.

***m^** and *μ*.** High m^* is favorable to get high S^2n. Nevertheless, most materials having high m^* usually has low μ, therefore, the power factor (*PF*) was limited by a weighted mobility, defined as $\left(m^*\right)^{3/2}\mu$. This limit could be broken if the carrier scattering mechanism turns from normal acoustic phonon scattering (r=-1/2, $\mu \propto \left(m^*\right)^{-1}$) to ionized defect scattering (r=+3/2, $\mu \propto \left(m^*\right)^{+1}$) [44], r is the scattering parameter. One way to achieve modification of relaxation time of mobile carrier is by using the resonant scattering, as suggested by Ravich [45].

***κ_{lat}* and *μ*.** Most strategies to reduce lattice thermal conductivity come with some tradeoff in carrier mobility because most defects, such as atomic defect, dispersed particle, and grain boundary, scatter not only phonons but also electrons. The improvement of *ZT* is therefore determined by the ratio of μ/κ_{lat}. Although an increase in the μ/κ_{lat} ratio is usually experimentally achieved through a more reduction in κ_{lat} than that in μ, some fundamental issues are still not well understood [25]. The wavelength (λ) and mean free path (*mfp*) for phonons (or electrons) at certain energy are unknown for most materials system, making the theoretical predication of thermal conductivity (electronic conductivity) extremely difficult for nanocomposite with varying-size inclusions. Because the wavelength span of phonons is much wider than that of electrons, the λ could span from 0.01 to 100 μm for phonons, while from several to hundreds of unit cells for electrons. Since the velocity of phonons (or electrons) does not change too much regarding to the energy, the wider λ span for phonons is therefore leading to wider span of *mfp*. The precise understanding of the distribution λ and *mfp* of phonons (electrons) contributing to the thermal conductivity (electrical conductivity) is a key step to tune the size and concentration of inclusions in nanocomposites to maximize the μ/κ_{lat} ratio.

Wiedemann-Franz law. The Wiedemann–Franz law states that the electronic contribution to the thermal conductivity is proportional to the electrical conductivity of materials according to the relationship $\kappa_{carr}=L\sigma T$, where L is the Lorenz number. The Lorenz number is within a range of 1.6-2.2 x10^{-8} V^2/K^2 for most thermoelectric materials, depending on the Fermi

energy and scattering parameters. A recent theoretical study shows that as the case of transport distribution being bounded, a rectangular-shape peaked electronic density of states approaching a Dirac delta function [46] . A recent theoretical study shows that the transport distribution function is bounded, a rectangular-shape distribution is instead found to be more favorable one to obtain the high *ZT* value because of with appropriate violations of the Wiedemann-Franz law, which could be achieved through nanoroute [47].

Bipolar effect. For most narrow semiconductor, thermal excitation of carrier from valance band to conduction band generates two kinds of carriers: hole and electron. The thermal excitation usually does not change the concentration of major carrier too much, but increase the minor carrier concentration (with an opposite sign to major carrier) significantly. Bipolar effect takes place when two types of carrier are present [48]. However, bipolar effect is notorious to achieve effective thermoelectric power generation. The first impact of bipolar is that the heat was stolen from hot-side to cold-side even if there is no net current, the origin of $\kappa_{bipolar}$. The second impact of bipolar is that Seebeck coefficient is suppressed by the simultaneous presence of two types of carriers with opposite sign of electronic charge. For n-type materials under non-degeneration condition, $\kappa_{bipolar}$ can be explored as [49],

$$\kappa_{bipolar} = \sigma_e T \left(\frac{k_B}{e} \right)^2 \left(\frac{\left(2r + 5 + \eta_g \right)^2}{1 + e^{\eta_f} e^{\eta_g} \left(m_e^* / m_h^* \right)^{3/2} \left(\mu_e / \mu_h \right)^{3/2}} \right), \tag{2}$$

where the k_B, e, η_f, η_g are the Boltzman constant, free electron charge, reduced Fermi energy E_f/k_BT, and reduced band gap E_g/k_BT, respectively. The subscripts e and h mean electrons and phonons, respectively.

The bipolar effect in a n-type material could be restrained by increasing the external carrier concentration (i.e., via raising the Fermi energy E_f), enlarging the band gap E_g and increasing the ratio of m_e^* / m_h^* or μ_e / μ_h. Normally an increase in external carrier concentration will decrease the Seebeck coefficient and an increase in the band gap will decrease the carrier mobility. The increase in ratio of m_e^* / m_h^* for n-type (m_h^* / m_e^* for p-type) could be realized by changing DOS of conduction band (valence band). A more viable way is to introduce some selective scattering to the minor carriers, i.e., holes to n-type while electrons to p-type materials,

to increase the ratio of μ_e / μ_h for n-type while μ_h / μ_e for p-type materials. The observation of obviously reduced bipolar effect in the p-type $Bi_xSb_{2-x}Te_3$ nanocomposite could be resorted to the selective scattering of electrons rather than holes by grain boundaries [50].

3. Selected thermoelectric nanocomposites

Thermoelectric materials comprise a huge family, including different material systems from semimetal, semiconductor to ceramic, covering various crystalline forms from single crystal, polycrystal to nanocomposite, and containing varying dimensions from bulk, film, wire to cluster. Recently, some polymer also shows interesting thermoelectric properties [51], however, it is not the topic of this review. Our goal herein is to update the new advancement in some selected bulk nanocomposites for potential thermoelectric power generation applications with a special focus on the half-Heslser system which has been less reviewed previously and also to shed some lights on the new advances of traditional systems: $CoSb_3$, PbTe, and Bi_2Te_3.

3.1. Half-Heuslers

Half-Heuslers with the general formula ABX refer to a wide family of compounds, which crystallize in the cubic structure and get their reputation for high temperature thermoelectric power generation owing to their high temperature stability as well as abundance [52]. Figure 2 shows the ideal $F\bar{4}3m$ half-Heusler ABX and the reported elements for the A, B and X sub-lattices and the partial periodical table. The structure of half-Heusler could be understood as a simple rock salt structure formed by A and X, and filled with element B at the one of the two body diagonal positions (1/4, 1/4, 1/4) in the cell, leaving the other one (3/4, 3/4, 3/4) unoccupied [53]. If both body diagonal positions in the cell are filled by the element B, it is called full-Heusler which is usually metallic. For the past decade, most research has been focused on the system ACoSb (A= Ti, Zr, and Hf) for p-type [16][55][56][57][58] and ANiSn (A=Ti, Zr, and Hf) for n-type [17][52][54][59], with limited attention on other systems, such as NbCoSn [60], VFeSb [61], etc. Traditionally, the isoelectronic substitution by other atoms at A-site [58] [62] [63][64] or B-site [65] [66] was used to maximize the alloying scattering to the phonon and slightly doping elements at X-site were employed to adjust the carrier concentration

[55][64]. There have been some experiments about tuning the carrier concentration by doping Nb [67][68], Y [69], V [70], Ta [71], Mn [72] or La [73] at A-site. However, the ZT value of half-Heusler remains quite low for a long time, only 0.5 at 1000 K in p-type $Hf_{0.5}Zr_{0.5}CoSb_{0.8}Sn_{0.2}$ [62] and 0.8 at 1025 K for n-type $Hf_{0.75}Zr_{0.25}NiSn_{0.975}Sb_{0.025}$ [63] was reported due to high lattice thermal conductivity (4~5 W/mK). Recently, a breakthrough was achieved in both p-type and n-type half-Heuslers by our groups [16][17]. The notable improvement in *ZT* value, 60% improvement to 0.8 in p-type $Hf_{0.5}Zr_{0.5}CoSb_{1-x}Sn_x$ and 25% increment to 1.0 in n-type $Hf_{0.75}Zr_{0.25}NiSn_{1-x}Sb_x$, benefited from the formation of half-Heusler nanocomposite through a high energy ball milling combined with a dc-current assisted hot pressing.

Since the direct synthesis of $Hf_{1-x}Zr_xCoSb$ and $Hf_{1-x}Zr_xNiSn$ is difficult by simply mechanical alloying, arc melting was first used to synthesize the ingot. Following that, mechanical ball milling was employed to get the nano powders, which were then compacted into bulk by fast hot pressing. Figure 3 shows the typical TEM images of $Hf_{1-x}Zr_xCoSb$ and $Hf_{1-x}Zr_xNiSn$ nanocomposites. Both $Hf_{1-x}Zr_xCoSb$ and $Hf_{1-x}Zr_xNiSn$ nanocomposites show an average grain size about 100-300 nm, as shown in Fig. 3 (a) and (b). Besides the fine grain size, some other noticeable features contained in both $Hf_{1-x}Zr_xCoSb$ and $Hf_{1-x}Zr_xNiSn$ nanocomposites are the widely-distributed nano inclusions with size ranging from 5 to 30 nm. Figure 3(c) shows a typical nano inclusion with a size of 10 nm in p-type $Hf_{1-x}Zr_xCoSb$. Close energy dispersive spectroscopy (EDS) examination indicates that composition of the nano inclusions is different from that of the surrounding matrix. Such nano inclusions embedded in matrix due to composition fluctuation has been experimentally proved to significantly scatter the long-wavelength phonons while has only slight adverse impact to the carrier transport in $AgPb_mSbTe_{m+2}$ system [7]. Therefore, a similar effect is expected in $Hf_{1-x}Zr_xCoSb$ and $Hf_{1-x}Zr_xNiSn$ nanocomposites. Additionally, a distorted lattice was observed in n-type $Hf_{1-x}Zr_xNiSn$, as shown in Fig. 3(d), which has also been considered as another phonon scattering mechanism.

Figure 4 shows the temperature-dependent Seebeck coefficient, thermal conductivity and ZT value for the p-type $Hf_{1-x}Zr_xCoSb$ and n-type $Hf_{1-x}Zr_xNiSn$ nanocomposites. Due to the strong phonon scattering by the grain boundaries, nano inclusion, and distorted lattice, κ_{lat} of nanocomposites at room temperature is much lower than that of their ingot counterpart, 29%

reduction from 4.1 $Wm^{-1}K^{-1}$ to 2.8 $Wm^{-1}K^{-1}$ for p-type $Hf_{1-x}Zr_xCoSb$ (Fig. 4(c)) and 22.5% reduction from 4.0 $Wm^{-1}K^{-1}$ to 3.1 $Wm^{-1}K^{-1}$ for n-type $Hf_{1-x}Zr_xNiSn$ (Fig. 4(d)). Another noteworthy phenomenon is that an enhanced Seebeck coefficient is observed for both p-type $Hf_{1-x}Zr_xCoSb$ and n-type $Hf_{1-x}Zr_xNiSn$ nanocomposites, as shown in Fig. 4(a) and 4(b). Such enhanced Seebeck coefficients with reduced electrical conductivity indicates a decreased carrier concentration. Normally, the decreased carrier concentration leads to a lowering of the Fermi energy and a rising of the thermal conductivity at the lower temperature due to the bipolar effect, as indicated by the Equation (2). The temperature-dependent thermal conductivity of n-type $Hf_{1-x}Zr_xNiSn$ nanocomposite obeys such normal behavior, as shown in Fig. 4(d). However, p-type $Hf_{1-x}Zr_xCoSb$ nanocomposite shows the opposite trend, suppressed increasing rate of thermal conductivity as compared with their ingot counterpart. This is a direct evidence of energy filtering effect, which shows an equivalent effect to an enlarging bang gap. Such filtering effect due to the grain boundary was also been observed in p-type $Bi_{1-x}Sb_xTe_3$ nanocomposite [50]. Nevertheless, we have very limited knowledge about the working mechanism of such filtering effect owing to the grain boundary or other special nano inclusions. How to control or tune the potential barrier to optimize the thermoelectric transport properties still presents a serious challenge. Due to remarkable reduction in κ_{lat}, a 25% improvement in peak *ZT* from 0.8 to 1.0 at 600 ^oC-700 ^oC has been achieved in n-type $Hf_{0.75}Zr_{0.25}NiSn_{0.99}Sb_{0.01}$. Further, the combining benefits from both the reduced κ_{lat} and suppressed $\kappa_{bipolar}$ enables a 60% improvement from 0.5 to 0.8 in p-type $Hf_{0.5}Zr_{0.5}CoSb_{0.8}Sn_{0.2}$ as it goes from normal ingot to nanocompoiste.

The κ_{lat} of half-Heuslers is greatly suppressed by reducing the average grain size from several micrometers to 100-200 nm and introducing some nano inclusions through a simple ball milling and hot pressing route. However, thermal conductivity of half-Heuslers is still much higher than that of conventional thermoelectric materials, such as Bi_2Te_3-based or PbTe-based nanocomposites. Normally, the grain boundary scatters not only the phonons but also the electrons. However, in both $Hf_{1-x}Zr_xNiSn$ and $Hf_{1-x}Zr_xCoSb$, no considerable decrease in the carrier mobility was observed as they go from the ingot with average grain size of several micrometers to nanocomposite with average grain size of 100-200 nm. Therefore, we propose that a further enhancement is reachable in both $Hf_{1-x}Zr_xNiSn$ and $Hf_{1-x}Zr_xCoSb$ if we can continuously reduce the grain size down to 30-50 nm, or even smaller. We also noted that the grain size of ball milled nanopowders is only 5-10 nm while most of such nano grains are

aggregated into particles with a size of several hundred nanometers. If we could break these agglomerates into narrowly-dispersed atomic-clusters with a size of 5-10 nm, the grain growth in the hot pressing process is more likely to be easily inhibited and smaller grain size is expected in the final nanocomposite bulk. An alternative fabrication method to make the nano powders is melt spinning, which is known to get amorphous powders by using the rapid quenching on a copper roller rotating in a high speed and has been applied to the half-Heusler system [74]. It is worthy to point out that powders made from melt spinning is not the narrowly-dispersed nanopowders but powder mixture with a size ranging from several nanometers to micro meters [5]. There have been some other efforts to introduce some incoherent nanoinclusions, such as InSb [75] and NiO [76]. By in-situ forming InSb nanoinclusions inside (Ti, Zr, Hf)(Co, Ni)Sb matrix, Xie et al. has achieved ZT~0.5 at 820 K for the sample containing 1 at.% InSb nanoinclusions. Very interestingly, the researchers at University of New Orleans present a novel nano inclusion by adding excess Ni in $Hf_{1-x}Zr_xNi_{1+\delta}Sn$ to form full-Heusler phase into the half-Heusler matrix, and claim a significant reduction in lattice thermal conductivity [77].

Another way to further depress the κ_{lat} of half-Heuslers is through enhancing the alloy scattering. In principle, larger differences in atomic mass and size would generate substantial local stress and hence strong phonon scattering, leading to lower lattice thermal conductivity. It has been experimentally confirmed that the κ_{lat} of $Hf_{0.5}Ti_{0.5}NiSn$ is much lower than that of $Hf_{0.5}Zr_{0.5}NiSn$ [78]. Enlightened by both theory and experiment, more work on binary combination of Hf and Ti or even ternary combination of Hf, Zr, and Ti in p-type half-Heuslers should be carried out. Additionally, an alternative co-doping approach, which involves substituting the Co in TiCoSb with equally Ni and Fe [79], was also been used to reduce the lattice thermal conductivity. Such strategy to substitute one element with one neighbor element with few valence electrons and another neighbor element with more valence electrons, has proved effective in Ag and Sb co-doped PbTe [7], and Te and Sn co-doped $CoSb_3$ [14]. Co-doping strategies at both B-site and X-site may be a new direction for the ABX-type half-Heusler systems. According to systematic calculations [53], besides the besides the (Ti, Zr, Hf)CoSb, (Ti, Zr, Hf)NiSn, (V, Nb, Ta)CoSn and (Sc, Y, La)NiSb, other promising yet less investigated half-Hesulers are NbCoSn, NbRhSn, ZrCoBi, VFeSb, NdFeSb for p-type materials and LaPdBi, NdCoSn, YNiSb, ZrCoBi for n-type naterials.

3.2 Skutterudites

Skutterudites, with a general formula MX_3 (M=Co, Rh, Ir; X=P, As, Sb), attract wide attention from the thermoelectric community due to their special lattice structure: an X_{12}-icosahedral nano-cage at 2a site (0, 0, 0), as shown in Figure 5. Adding one heavy metal atom (R) into the intrinsic nanocage forms the filled skutterudites: $R_xM_4X_{12}$. The loose bonding of guest atoms with the host lattice generates local vibrational modes that strongly scatter the phonon transport, one phenomenon also known as the "rattling effect" [80]. Such an idea initiated a wide investigation of filling elements to the cage-site, including most of rare earth, alkaline earth, and alkali metal elements for both n-type $R_xCo_4Sb_{12}$ and p-type $R_xFe_{4-y}Co_ySb_{12}$. Theoretical study demonstrated that the filling fraction of doping element in cage-site of $R_xCo_4Sb_{12}$ is associated with the electronegativity difference between the filling atom R and host lattice atom Sb [81]. Only the element satisfying the electronegativity difference relationship, i.e., X_R-X_{Sb}<0.8, could get into the cage site of $R_xCo_4Sb_{12}$. This filling fraction limit can be removed by adding some electron-charge-compensation elements, such as doping Fe at Co-site, or doping Sn and Ge at Sb-site.

The vibration modes generated by the rattling atoms in skutterudites were identified as local harmonic vibrational modes, or Einstein modes, by inelastic neutron scattering measurements and phonon density-of-state calculation. An inelastic scattering mechanism was proposed to explain the energy interaction between the lattice phonon and the localized phonons [82]. According to the proposed mechanism, the local phonons may first absorb a small amount of energy from the lattice phonons to get into an excited rattling state, and then later release the energy back to the lattice phonons with wave vectors incoherent with those of the absorbed phonons. Therefore, only the lattice phonons with energy similar to that of the local phonons would be impacted, and such phonon scattering mechanism was also named as resonant phonon scattering [83]. Normally, the resonant frequency ω_0 of modes in a simply ball-spring picture is related to the mass of ball mass m and the elastic constant k of spring through the relationship $\omega_0=(k/m)^{1/2}$. By conducting ab initial calculation, the spring constant k of filler R in filled skutterudite can be obtained by applying the relationship of $E=1/2kx^2$, where E is the change of total energy and x the displacement of R using the cage center as the reference point. According to Yang *et al*.'s calculation [84], fillers with similar chemical characteristics demonstrate similar

ω_0, while filler atoms from different groups show considerably different ω_0. Consequently, the κ_{lat} of multi-filled skutterudites with fillers from different groups could be lower than that of single-filled skutterudites. Figure 6 shows the lattice thermal conductivities of typical single-, double- and triple- filled skutterudites at 300 K and 850 K, respectively [18]. A remarkable reduction in lattice thermal conductivity was observed in skutterudites when it goes from single-, to double-, to tripled-filled materials. The lattice thermal conductivity of triple-filled $Ba_uLa_uYb_wCo_4Sb_{12}$ is 1~2 $Wm^{-1}K^{-1}$ at 300 K and ~0.2 $Wm^{-1}K^{-1}$ at 850 K. A minimum thermal conductivity was estimated of 0.45 $Wm^{-1}K^{-1}$ by using the equation $k_{min}=1/3C_v v l_{min}$, where C_v is the specific heat per volume, v is the sound velocity, and l_{min} is the minimum phonon mean free path, equal to the nearest interatomic distance. It is clear that the observed k_L (~0.2 $Wm^{-1}K^{-1}$) is much lower than the theoretical value, which is based on a random walk between Einstein oscillators of varying sizes through subdividing the sample volume into subgroups of atoms. Shi *et al*. [18] resolved such dilemma by considering the oscillator as sole individual, used half of the nearest interatomic distance (1.26 Å), and finally reached a new limit value, κ_{Eins}, of 0.23 $Wm^{-1}K^{-1}$. It is worthy to point out that the 0.2 $Wm^{-1}K^{-1}$ at 850 K given by Shi *et al*. may be underestimated by using a constant Lorenz number of 2.0 $x10^{-8}V^2K^{-2}$ for the whole temperature range. Even there are still some arguments on the real κ_{lat} at high temperature, the multiple-filling really reduces κ_{lat}, and ZT thus reaches a new milestone value of 1.7 at 850 K for n-type $Ba_{0.08}La_{0.05}Yb_{0.04}Co_4Sb_{12}$ [18] and 1.3 at 800 K for $Sr_{0.12}Ba_{0.18}DD_{0.39}Fe_3CoSb_{12}$ (p-type) [10]. Optimizing the combination of various fillers may achieve a further improvement. Since most of the pure rare earth elements are expensive, some much cheaper rare earth mixtures are natural multiple fillers, such as DD (Didymium, 4.76 mass% Pr and 95.24 mass% Nd) and Mm (mischmetal, La 50.8%, Ce28.1%, Nd16.1%, Pr5.0%), may point out some more cheaper way to make multi-filled skutterudites [85][86]. Recently, Mona *et al.* [87] conducted a two-dimensional model, which consists of host atoms on a rectangular lattice with filler at the center. The effect of mass and size of the filler on κ_{lat} is investigated using equilibrium molecular-dynamics simulation. It is shown that (1) the κ_{lat} decrease with increasing atomic displacement parameter; (2) the κ_{lat} has alocal minima versus the filler to host mass. Surprisedly, similar trend was observed in experiment on filled-skutterudites. This work gives us a new way to understand the mechanism behind the reduced κ_{lat} in filled skutterudites.

Besides manipulating the fillers in the intrinsic nanocages of skutterudties, a co-doping strategy, by substituting Sb in $CoSb_3$ with Te and IVB group element simultaneously, was developed to reduce the lattice thermal conductivity [14]. Due to a considerable decrease in lattice thermal conductivity, Te and Sn co-doped $CoSb_{2.70}Te_{0.25}Sn_{0.05}$ records a ZT of 1.1 at 550 ^oC in unfilled skutterduites. The high resolution TEM image demonstrates some nano inclusions inside grains which are similar to those observed in LAST system. The presence of nanoinclusions has been considered an effective route to scatter the phonons in $AgPb_mSbTe_{m+2}$ system [7]. Figure 7 shows the Raman shift of $CoSb_{2.86}M_{0.02}Te_{0.12}$ (M=Sb, Si, Ge, Sn, Pb). The main peaks observed at 130.4, 150.2, 176.5, and 183.5 cm^{-1} are in good agreement with the phonon modes predicated by the theoretical calculation. The $CoSb_{2.86}Si_{0.02}Te_{0.12}$ and $CoSb_{2.86}Pb_{0.02}Te_{0.12}$ samples display similar Raman response patterns to $CoSb_{2.88}Te_{0.12}$, while $CoSb_{2.86}Ge_{0.02}Te_{0.12}$ and $CoSb_{2.86}Sn_{0.02}Te_{0.12}$ show significant differences. The most remarkable change is the shift of most peaks towards the lower frequency as well as a new peak which appeared at ~167.3 cm^{-1} and possibly resulted from the change by one of the F_{g3}, F_{g4} and A_{g2} modes, or from the splitting of one degenerate vibration mode because of the broken symmetry of Sb_4 rings as Sn/Te, or Ge/Te get into the Sb_4 rings. Recently, the impact of Ge/Te co-doped $CoSb_3$ were investigated [88][89], and a Ge/Te-rich nano dots was also observed [90]. The nanostructure observed in Te/Sn and Te/Ge co-doped samples could be attributed to the phase segregation of $CoTe_{1.5}M_{1.5}$(M=Ge, Sn) from the matrix $CoSb_3$. Such kind of phase segregation was also achieved by partially substituting Co with Ir in $Ba_{0.2}(Co_{1-x}Ir_x)_4Sb_{12}$ following a long time annealing, resulting in a 27% reduction in κ_{lat} in $Ir_{0.2}$ sample [91]. A molecular dynamics calculation done by Kim *et al*. indicated that the filled skutterudites can also greatly benefit from the presence of order-disorder phase transitions of fillers in the voids of skutterudites structure. A minimum lattice thermal conductivity has been predicted in the two-phase mixture region, considering a dominant scattering of the long-range acoustic phonon [92]. There are also some other strategies to form some nano particles at grain boundary of $R_xCo_4Sb_{12}$ through in-situ oxidation or reaction [93][94][95], or to in-situ synthesize nano/micro-meter composites [96].

3.3 PbTe, PbSe, PbS, $AgSbTe_2$

PbTe and its alloys have been leading a dominant role in the thermoelectric power generation application for more than 50 years, especially in the deep space exploring program. A broad fundamental investigation has been carried out in Soviet and USA regarding exploring applications of PbTe system. However, a reliable high temperature thermal conductivity measurement of semiconductor remains a challenge until the advent of the laser flash method, leading to a underestimated ZT value of 0.8 for p-type Na-doped PbTe and 0.7 for n-type I-doped PbTe for a long time. Recently, the researchers at California Institute of Technology conducted a careful re-investigation of both n- and p-type PbTe [97][98]. Laser flash technique was used for thermal diffusivity measurement up to 800 K and resulted in significantly lower thermal conductivity values than previous estimates. The combination of precise control of the doping level and reliable thermal conductivity measurements resulted in a large figure of merit of 1.4 for both n- and p-type PbTe, as shown in Fig. 8. Embedding some coherent or incoherent nanoinclusions into the matrix has been widely confirmed as an effective approach to reduce the lattice thermal conductivity. The difference between coherent and incoherent involves the degree of lattice alignment between the matrix phase and the nanoinclusion [99]. The coherent nanoinclusion usually refers to the situation that the dispersed phase has a similar lattice parameter and shows a good lattice alignment with the matrix phase, while an incoherent nanoinclusion is related to a clear boundary between the matrix phase and dispersed phase. Figure 9 summarizes the reduced lattice thermal conductivity of PbTe-based nanocomposite with various nanoinclusions, including Bi [100], Pb [100], Sb [100], SrTe [12], $AgSbTe_2$ [7], $NaSbTe_2$ [101], PbS [102], CdTe [103], and Ag_2Te [104]. Both the coherent and incoherent nanoinclusions could significantly reduce the lattice thermal conductivity. However, the phonon scattering mechanism is different to certain degree. Firstly, the stress level of coherent boundary is higher than that of incoherent boundary. The scattering to phonon at coherent boundary comes from the centralized stress due to the slightly mismatched lattice, showing a similar effect with the point defect. However, for the incoherent boundary, the mismatched phonon modes are responsible for the reduced lattice thermal conductivity. Due to the size confinement, the phonon with a wavelength larger than the dispersed phase would be filtered out. In other words, the long wavelength phonon could not pass through the nano particles due to a phonon filter effect. Although incoherent nanoinclusions could reduce lattice thermal conductivity significantly, they

also have notable negative impact on the electrons transport. This is why high ZT values of 1.7~1.8 is obtained in the PbTe nanocomposite with coherent nanoinclusions $AgSbTe_2$ [7], $NaSbTe_2$ [101], SrTe [12], etc. while only 1.4~1.5 is obtained in PbTe nanocomposite with incoherent nanoinclusions Sb [100] and Ag_2Te [104], etc. Besides manipulating the various nano structures, the band structure engineering could also help a lot to improve the power factor. Recently, Pei *et al*. found that a convergence of electronic band in $PbTe_{1-x}Se_x$ could achieve increased carrier mobility without negative impact to carrier mobility, and finally a ZT of 1.8 was achieved in heavily doped $Na_{0.02}Pb_{0.98}Te_{0.85}Se_{0.15}$ [12].

Since Te is very rare in the Earth's crust (0.001 ppm), even less than Pt (0.005 ppm) and Au (0.004 ppm), it is desirable to develop some alternative material with less Te involved. PbSe and PbS, which show similar rock salt structure to PbTe while slightly larger band gap, also get attention recently. Wang *et al*. reported a ZT value of 1.2 at 850 K in Na-doped p-type PbSe [13], which is slightly lower than 1.4 for Na-doped p-type PbTe. Recently, Zhang *et al*.[15] achieved a ZT of 1.3 at 850 K in Al-doped n-type PbSe, which is comparable to 1.4 for I-doped n-type PbTe. It was found that Seebeck coefficient of Al-doped PbSe was about 40%-100% higher than the value predicted by a simple parabolic model and was also higher than that of the Cl-doped PbSe reference sample. An additional resonant state was claimed to be induced in the conduction band by doping some Al into PbSe, similar to the effect of Tl in PbTe [38]. By embedding some PbS nano particle into the PbSe matrix, a ZT of 1.2~1.3 was obtained in Cl-doped PbSe due to a reduced lattice thermal conductivity. In contrast to PbSe, only moderate ZT of 0.8 at 900 K was obtained in PbS even with some PbTe nanoinclusion [105]. $AgSbTe_2$, which crystallizes into cubic structure, is known to possess extremely low lattice thermal conductivity. The intrinsic low lattice thermal conductivity comes from an extreme anharmonicity of the lattice vibrational spectrum that gives rise to a high Grüneisen parameter and strong phonon-phonon interactions owing to the random distribution of Ag and Sb in the same lattice site [106]. As a result, ZT of 1.5 has been reported in stochimetric $AgSbTe_2$ made by chemical alloying [107] or by physical alloying [108] method, respectively.

3.4 Bi_2Te_3

Bi_2Te_3-based materials, with a lamellar structure perpendicular to the c-axis, have been studied as near room temperature thermoelectric materials since 1960s, and now dominate the market of thermoelectric refrigerator. The potential application in solid state solar thermoelectric power generator initiates another life for this material system. Even conventional polycrystalline Bi_2Te_3-based materials have slightly lower ZT value but much better mechanical property than their single crystalline counterpart, still showing an advantage for wide industry applications. Recently, the nanocomposites synthesized by high-energy ball milling combined with dc-current assisted hot pressing [50] and melt-spinning together with spark plasma sintering [5], respectively, pushed the ZT value of p-type $Bi_xSb_{2-x}Te_3$ up to 1.4~1.5 from 1.0 of their ingot counterpart. The improvement arises from the introduction of phonon scattering centers with different size scales from nanoinclusion to grain boundary, as demonstrated by the TEM observations. However, no obvious improvement was obtained when such simple fabrication technologies were applied to n-type $Bi_2Te_{3-x}Se_x$. The gain from the decrease in κ_{lat} was canceled by the simultaneous decrease in power factor due to a decrease in carrier mobility and an increase in carrier thermal conductivity owing to increased carrier concentration. The higher anisotropy of electronic transport in n-type $Bi_2Te_{3-x}Se_x$ than in p-type $Bi_2Sb_{2-x}Te_3$, finally leads to the lower average mobility in polycrystalline n-type samples with randomly oriented grains than that of single crystals grown along the basal plane. Aligning the random-oriented grains into ordered grains by flowing perpendicular to pressure [109] [110] or extruding parallel to pressure [111] has been experimentally confirmed as an effectively route to get higher power factor. Another side effect to impede the advancement of n-type $Bi_2Te_{3-x}Se_x$ made by the powder metallurgy method, is the Te-vacancy generated from mechanical deformation or from the evaporation of Te. Te vacancy, n-type donor and difficult to control, usually generates a repeatability issue. The repeatability issue does not deteriorate the peak ZT, but results in always varying electrical conductivity which reduces the device efficiency. A significant improvement on repeatability from batch to batch processing of $Bi_2Te_{2.7}Se_{0.3}$ was achieved by adding a small amount of Cu. The reason for such improvement is that Cu gets into the interstitial site to suppress the escape of Te atoms, as a result, leading to a less Te vacancy fluctuation from batch to batch. Such experimental result reverses the normal understanding for the role Cu plays. In industry, Cu is usually used as electrode for Bi_2Te_3-based thermoelectric devices, and is also

harmful to the thermoelectric properties of Bi_2Te_3-based thermoelectric materials since copper can easily diffuse along the basal plane of Bi_2Te_3 lattice and work as very strong donor impurity. A blocking layer such as Ni was usually introduced to separate the Cu electrode and Bi_2Te_3 matrix [112]. However, an appropriate amount of copper atoms located in the interstitial site between the van der Waals bounded layers of Bi_2Te_3-based materials could work as electronic connection between these weakly connected layers. Consequently, an increase in carrier mobility was observed in copper-doped $Bi_2Te_{2.7}Se_{0.3}$ polycrystals, ZT of 0.94~0.99 is achieved in $Cu_{0.01}Bi_2Te_{2.7}Se_{0.3}$ ploycrystal, higher than the value of 0.85 in $Bi_2Te_{2.7}Se_{0.3}$ with comparable carrier concentration. Additionally, the improved ZT value also benefits from the reduced lattice thermal conductivity, which is related to novel nano stress stripes that parallel to the basal plane as shown in Fig. 10(a) and (b). Figure 10 (c) and (d) show some Cu nano particles observed in high copper content sample $Cu_{0.07}Bi_2Te_3$ by Han *et al*. Such metal precipitations have also been considered the effective approach to reduce the lattice thermal conductivity [113].

Besides the phonon scattering observed in metal particle dispersed nanocomposite, a carrier filtering effect in Pt/Sb_2Te_3 nanocomposite has been claimed by Ko *et al*. [114]. A significant increase in Seebeck coefficient from 115.6 to 151.6 μVK^{-1} was achieved through the filtering effect of lower energy carriers owing to the introduction of Pt nano particle into Sb_2Te_3 matrix. The filtering effect has an equivalent effect to increase the band gap and hence reduce the negative impact of bipolar effect in the intrinsic region. Liu *et al*. systematically investigated the effect of SiC nano particle on the thermoelectric transport of both n-type and p-type Bi_2Te_3-based alloys. The addition of SiC nano particle slightly increased the power factor of p-type Bi_2Te_3 while decreased the power factor of n-type Bi_2Te_3. Hall measurement demonstrates that the addition of 1% SiC raises the carrier concentration by 100% 1.0 time for n-type while by 1.5 150% times for p-type, and reduce the carrier mobility greater in n-type (to about 1/10) than in p-type (to about 1/2). The carrier concentration changes could be attributed to the generation of Te-vacancy in $Bi_2Te_{2.7}Se_{0.3}$ and Sb-antisite in $Bi_{0.5}Sb_{1.5}Te_3$ due to the addition of SiC. The difference in reduced carrier mobility revealed that SiC nano particles scatter electrons rather than holes in Bi_2Te_3-based materials. Such selective scattering is useful to reduce the bipolar effect through the ratio of μ_e/μ_h [115].

Additionally, there are also some strategies conducted on grain boundary to tune the thermoelectric properties. Ji *et al*. [116] reported that a 30~38% improvement in power factor of p-type Bi_2Te_3 system by utilizing an alkali metal salt hydrothermal nano-coating treatment approach. Zhang *el al*. [117] recently conducted a grain boundary modification to suppress the grain growth of p-type $Bi_{0.4}Sb_{1.6}Te_3$ by adding some oleic acid into the materials before ball milling process. The average grain size of $Bi_{0.4}Sb_{1.6}Te_3$ is successfully reduced from 2~3 μm down to 200~500 nm, finally resulting in a lower lattice thermal conductivity. These grain boundary engineering pave a new way to enhance the *ZT* value.

4. What is the new direction?

We have witnessed remarkable advancements in material synthesis, microstructure characterization, physical properties measurement, and theoretical understanding for thermoelectric materials. Most fruitful results come from the concept of nanocomposite, which characterizes as a material consist of nano grains, defects in the grains, nanoinclusions, and particles randomly dispersed. The continuous effort has pushed the κ_{lat} of several systems very close to the theoretical limit by combining several scattering centers with varying sizes from nano to micro scale, unfortunately, with a sacrifice in carrier mobility. The deteriorated carrier mobility resulted from the disturbance of various phonon scattering centers. In order to increase mobility μ without raising κ_{lat}, reconstructing the electron transport channel is necessary. One example is re-orientating the random grains of n-type polycrystalline Bi_2Te_3 into aligned grains and leading to a significant increase in μ [108][110]. Another example is the modulation doping [26][118], characterized as a two-phase composite where dopants are incorporated into only one phase. By band engineering, charge carriers could be separated from their parent grains and move into un-doped grains, resulting in enhanced mobility of the carriers in comparison with uniform doping due to a reduction of ionized impurity scattering, and finally leading to a higher power factor. Therefore, some sort of ordering of the modulation doping atoms and nanoinclusions will greatly improve the ratio μ/κ_{lat} and finally raise the *ZT* value. Such ordered

inclusions and selected boundaries are well known in low dimension superlattice or quantum well structure, which allow high μ and low κ_{lat} achieved together with ZT>2 [119].

Here we propose some key characteristics for the new generation nanocomposites, called ordered nanocomposites, in contrast with those of the current dis-ordered nanocomposites, called random nanocomposite. We will explain these characters along size scale from doping atom, nanoinclusions, grain boundaries, grain shape, to void morphology as shown in Fig. 11.

Doping atom ----Modulation (Fig. 11(a)) vs. Uniform (Fig. 11(f))

Usually, thermoelectric materials are heavily doped semiconductors, and guest element is used to tune the carrier concentration with a reduction of carrier mobility due to a notable ionized impurity-electron scattering. For n-type material, the compound with open void lattice site, such as skutterudites and Clathrate, could have less impurity-electron scattering when external atom is doped at the void-site. While for the p-type, superlattice compound, such as Na_xCoO_3, shows much advantage over other structures due to its separated doping layer and transport layer. However, for most of other materials with such unique structures, a different strategy is available to minimize impurity-electron scattering, i.e., modulation doping. Modulation doping means that a two-phase composite with heavily doped minor-phase provides the carrier and non-doping matrix-phase as high speed transport channel [118] .

Nanoinclusion----Coherent (Fig. 11(b)) vs. Incoherent (Fig. 11(g))

The wide investigation of nano precipitation in PbTe system demonstrates that the coherent inclusion has less deteriorating effect on the carrier mobility than the incoherent inclusion. The theoretical study also indicates that the band structure modification due to such coherent nano inclusion [42][43]. By connecting with the concept of superlattice and quantum well in low dimensional systems, such coherent nanoinclusion is very useful to realize the superlattice or quantum well in three dimensions.

Random boundary (Fig. 11(c)) vs. Ordered boundary (Fig. 11(h))

The effect of grain boundary on the mechanical properties has been well studied in many materials. However, we only have limited understanding for the impact of grain boundary on the transport properties of most thermoelectric materials. Although there is a lack of statistic

understanding about the various grain boundaries and their impact on transport of phonons and electrons, it has been confirmed that some grain boundary has less impact on transport of electrons but still scatters phonons, such as twin boundary. Reconstructing the various random boundaries to some special ordered boundaries to facilitate the electrons transport will help increase the power factor significantly. The reorientation of n-type Bi_2Te_3-based polycrystals is an inspiring start point [109][110].

Unmodified grain (Fig. 11(d)) vs. Modified grain (Fig. 11(i))

Most thermoelectric materials crystallize in a cubic structure and are near-spherical in shape. As a result, both the thermal and electrical properties are isotropic in the polycrystalline sample. Concerning the transport behavior in nanowire (or film) along the in-line direction (or in-plane), the boundary confining effect has significantly scattering influence on phonons while slight influence on electrons. Since the grain boundary could have similar effect to confine the phonons along one direction to the surface to certain degree, to modify the spherical grain shape into plate-like or wire-like shape would be a new direction to decouple the transport of phonons and electrons.

Spherical void (Fig. 11(e)) vs. Columnar void (Fig. 11(j))

Within the scope of effective media theory, the normal void does not improve thermoelectric figure of merit ZT value. When it comes down to nano scale, limited improvement was observed. Recently, an inspiring work suggested that ordered nano holes could reduce the lattice thermal conductivity of silicon film close to the amorphous limit, but little impact on the carrier mobility, eventually enhancing the ZT value [120]. A theoretical study on the nanoporous silicon with varying size disorder at internal surface of hole will generate significant scattering to the phonons [121]. These works demonstrate bulk materials with columnar void would highly interesting for thermoelectric application. From the view point of fabrication technology, anode oxidized method has been successfully employed to make alumina with aligned column pores with size scale from tens of nanometers to hundreds of nanometers. However, making such tiny holes in current thermoelectric materials is a really challenge.

In summary, some significant advancement in thermoelectric figure-of-merit ZT has been made by nanocomposite approach in the past a few years, but still not good enough for broad

range of applications of thermoelectric technology displacing other technologies. It is certainly possible that more improvement can be achieved based on the current understanding. However, how to make the grains size in less than 50 nm in the final bulk materials is very challenging, but is really required for further improving ZT. Ordering of the nanostructures to create some sort of channels for the easy transport of electrons but difficult for the phonons will probably a fruitful direction for the future.

Acknowledgement: This work is supported by "Solid State Solar-Thermal Energy Conversion Center (S^3TEC)", an Energy Frontier Research Center founded by the U.S. Department of Energy, Office of Science, Office of Basic Energy Science under award number DE-SC0001299/DE-FG02-09ER46577 (GC and ZFR).

Reference

[1] BBC News, http://www.bbc.co.uk/news/business-12745899

[2] M. Grätzel, Inorg. Chem. 44 (2005)6841.

[3] G. L. Bennett, in: CRC Handbook of thermoelectrics, D. M. Rowe (Eds), CRC Press, Boca Raton, 1995, pp:515-537.

[4] D. M. Rowe, C. M. Bhandari, Modern thermoelectric, Reston Publishing Company, Inc., Reston, 1983.

[5] W. J. Xie, J. He, H. J. Kang, X. F. Tang, S. Zhu, M. Laver, S. Y. Wang, J. R. D. Copley, C. M. Brown, Q. J. Zhang, T. M. Tritt, Nano Lett. 10 (2010)3283.

[6] W. S. Liu, Q. Y. Zhang, Y. C. Lan, S. Shuo, X. Yan, Q. Zhang, H. Wang, D. Z. Wang, G. Chen, Z. F. Ren, Adv. Energy Mater. 1(2011)577.

[7] K. F. Hsu, S. Loo, F. Guo, W. Chen, J. S. Dyck, C. Uher, T. Hogan, E. K. Polychroniadis, M. G. Kanatzidis, Science 303(2004)818.

[8] G. H. Zhu, W. S. Liu, Y. C. Lan, G. Joshi, H. Wang, G. Chen, Z. F. Ren, Nano Energy, **2**, 1172-1178 (2013).

[9] J. S. Rhyee, K. Ahn, K. H. Lee, H. S. Ji, J. H. Shim, Adv. Mater. 23(2011)2191.

[10] B. Yu, Q. Y. Zhang, H. Wang, X. W. Wang, H. Z. Wang, D. Z. Wang, H. Wang, G. J. Snyder, G. Chen, Z. F. Ren, Journal of Applied Physics, 108(2010)016104.

[11] G. Rogl, A. Grytsiv, P. Rogl, E. Bauer, M. B. Kerber, M. Zehetbauer, S. Puchegger, Intermetalics18 (2010)2435.

[12] K. Biswas, J. Q. He, Q. C. Zhang, G. Y. Wang, C. Uher, V. P. Dravid, M. G. Kanatzidis, Nat. Chem.3(2011)160.

[13] H. Wang, Y. Z. Pei, A. D. LaLonde, G. J. Snyder, Adv. Mater. 23(2011)1366.

[14] W. S. Liu, B. P. Zhang, L. D. Zhao, J. F. Li, Chem. Mater. 20(2008)7526.

[15] Q. Y. Zhang, H. Wang, W. S. Liu, H. Z. Wang, B. Yu, Q. Zhang, D. Z. Wang, G. Ni, S. Y. Lee, G. Chen, Z. F. Ren, Energy Environ. Sci., 5(2012)5246.

[16] X. Yan, G. Joshi, W. S. Liu, Y. C. Lan, H. Wang, S. Y. Lee, J. W. Simonson, S. J. Poon, T. M. Tritt, G. Chen, Z. F. Ren, Nano Lett. 11(2011)556.

[17] G. Joshi, X. Yan, H. Z. Wang, W. S. Liu, G. Chen, Z. F. Ren, Adv. Energy Mater., 1(2011)643.

[18] X. Shi, J. Yang, J. R. Salvador, M. F. Chi, J. Y. Cho, H. Wang, S. Q. Bai, J. H. Yang, W. Q. Zhang, L. D. Chen, J. Am. Chem. Soc. 133(2011)7837.

[19] G. Joshi, H. Lee, Y. C. Lan, X. W. Wang, G. H. Zhu, R. W. Gould, D. C. Cuff, M. Y. Tang, M. S. Dresselhaus, G. Chen, Z. F. Ren,Nano Lett., 8(2008)4670.

[20] X. W. Wang, H. Lee, Y. C. Lan, G. H. Zhu, G. Joshi, D. Z. Wang, J. Yang, A. J. Muto, M. Y. Tang, J. Klatsky, S. Song, D. S. Dresselhaus, G. Chen, Z. F. Ren, Appl. Phys. Lett. 93(2008)193121.

[21] Q. F. Zhang, G. Z. Cao, Nano Today 6(2011)91.

[22] D. Kraemer, B. Poudel, H. P. Feng, J. C. Caylor, B. Yu, X. Yan, Y. Ma, X. W. Wang, D. Z. Wang, A. Muto, K. MacEnaney, M. Chiesa, Z. F. Ren, G. Chen, Nat. Mater. 10 (2011) 532.

[23] A. Shakouri, Annu. Rev. Mater. Res. 41(2011)17.1.

[24] GMZ energy, http://www.gmzenergy.com/

[25] A. J. Minnich, M. S. Dresselhaus, Z. F. Ren, G. Chen, Energy Environ. Sci. 2(2009) 466.

[26] P. Pichanusakorn, P. Bandaru, Mater. Sci. Eng. R 67(2010)19.

[27] D. L. Medlin, G. J. Snyder, Current Opinion in Colloid & Interface Science 14(2009)226.

[28] Y. C. Lan, A. J. Minnich, G. Chen, Z. F. Ren, Adv. Funct. Mater. 20(2010)357.

[29] J. F. Li, W. S. Liu, L. D. Chen, M. Zhou, NPG Asia Mater. 2(2010)152.

[30] C. J. Vineis, A. Shakouri, A. Majumdar, M. G. Kanatzidis, Adv. Mater. 22(2010) 3970.

[31] C. L. Wan, Y.F. Wang, N. Wang, W. Norimatsu, M. Kusunoki, and K. Koumoto, Sci. Tech. Adv. Mater. 11(2010)044306.

[32] H. Kleinke, Chem. Mater., 22(2010)604.

[33] E. S. Toberer, A. F. May, G. J. Snyder, Chem. Mater. 22(2010)624.

[34] M. G. Kanatzdis, Chem. Mater. 22(2010) 648.

[35] H. Ohta, K. Sugiura, and K. Koumoto, Inorg. Chem. 47(2008) 8429.

[36] J. R. Sootsman, D. Y. Chung, M. G. Kanatzidis, Angew. Chem. Int. Ed. 48(2009) 8616.

[37] L. F. Li, Z. Chen, M. Zhou, R. J. Huang, Front. Energy 5(2011)125.

[38] J. P. Heremans, V. Jovovic, E. S. Toberer, A. Saramat, K. Kurosaki, A. Charoenphakdee, S. Yamanaka, G. J. Snyder, Science 321(2008)554.

[39] Y. Z. Pei, X. Y. Shi, A. LaLonde, H. Wang, L. D. Chen, G. J. Snyder, Nature 473(2011)66.

[40] M. S. Dresselhaus, G. Chen, M. Y. Tang, R. G. Yang, H. Lee, D. Z. Wang, Z. F. Ren, J. P. Fleurial, P. Gogna, Adv. Mater. 19(2007)1043.

[41] H. Ohta, S. Kim, Y. Mune, T. Mizoguchi, K. Nomura, S. Ohta, T. Nomura, Y. Nakanishi, Y. Ikuhara, M. Hirano, H. Hosono, K. Koumoto, Nat. Mater. 6(2007)129.

[42] A. Popescu and L. M. Woods, Appl. Phys. Lett. 97 (2010)052102.

[43] Y. Zhang, X. Z. Ke, C. F. Chen, J. H. Yang, P. R. C. Kent, Phys. Rev. Lett. 106(2011)206601.

[44] W. S. Liu, L. D. Zhao, B. P. Zhang, H. L. Zhang, J. F. Li, Appl. Phys. Lett., 93(2008)042109.

[45] Y. I. Ravich, in: CRC Handbook of thermoeletrics, D. M. Rowe (Eds), CRC Press, Boca Raton,1995

[46] G. D. Mahan, J. O. Sofo, Proc. Nat. Acad. Sci. USA 93(1995)7436.

[47] Z. Y. Fan, H. Q. Wang, J. C. Zheng, J. Appl. Phys. 109(2011)073713.

[48] H. J. Goldsmid, Introduction to thermoelectricity, Springer, Heidelberg, 2009.

[49] W. S. Liu, B. P. Zhang, J. F. Li, H. L. Zhang, L. D. Zhao, J. Appl. Phys. 102(2007)103717.

[50] B. Poudel, Q. Hao, Y. Ma, Y. C. Chen, A. Minnich, B. Yu, X. Yan, D. Z. Wang, A. Muto, D. Vashaee, X. Y. Chen, J. M. Liu, M. S. Dresselhaus, G. Chen and Z. F. Ren, Sicence 320(2008)634.

[51] O. Bubnova, Z. U. Khan, A. Malti, S. Braun, M. Fahlman, M. Berggren, X. Crispin, Nat. Mater. 10(2011)429.

[52] S. J. Poon, in: Recent Trends in Thermoelectric Materials Research II, T. M. Tritt (Eds), Academic, New York, 2001.

[53] J. Yang, H. M. Li, T. Wu, W. Q. Zhang, L. D. Chen, J. H. Yang, Adv. Funct. Mater. 18(2008)2880.

[54] C. Uher, J. Yang, S. Hu, D. T. Morelli, G. P. Meisner, Phys. Rev. B, 59(1999)8615.

[55] Y. Xia, S. Bhattacharya, V. Ponnambalam, A. L. Pope, S. J. Poon, T. M. Tritt, J. Appl. Phys. 88 (2000) 1952.

[56] T. Sekimoto, K. Kurosaki, H. Muta, S. Yamanaka, J. Alloys Compd. 407(2006) 326.

[57] T. Wu, W. Jiang, X. Y. Li, Y. F. Zhou, L. D. Chen, J. Appl. Phys. 102(2007) 103705.

[58] V. Ponnambalam, P. N. Alboni, J. Edwards, T. M. Tritt, S. R. Culp, S. J. Poon, J. Appl. Phys. 103 (2008) 063716.

[59] H. Hohl, A. P. Ramirez, C. Goldmann, G. Ernst, B. Wolfing, E. Bucher, J. Phys.: Condens. Matter. 11(1999)1697.

[60] Y. Ono, S. Inayama, H. Adachi, T. Kajitani, Jpn. J. Appl. Phys. 45(2006)8740.

[61] M. M. Zou, J. F. Li, P. J. Guo, T. Kita, J. Phys. D, 43(2010)415403.

[62] S. R. Culp, J. W. Simonson, S. J. Poon, V. Ponnambalam, J. Edwards, T. M. Tritt, Appl. Phys. Lett. 93(2008) 022105.

[63] S. R. Culp, S. J. Poon, N. Hickman, T. M. Tritt, J. Blumm, Appl. Phys. Lett. 88(2006) 042106.

[64] W. J. Xie, X. F. Tang, Q. J. Zhang, Chin. Phys. 16(2007) 3549.

[65] N. J. Takas, P. Sahoo, D. Misra, H. F. Zhao, N. L. Henderson, K. Strokes, P. F. P. Poudeu, J. Electron. Mater. 40(2011) 662.

[66] P. Maji, N. J. Takas, D. K. Misra, H. Gabrisch, K. Stokes, P. F. P. Poudeu, J. Solid State Chem. 183(2010) 1120.

[67] P. J. Lee, L. S. Chao, J. Alloys Compd. 504(2010) 192.

[68] H. Muta, T. Kanemitsu, K. Kurosaki, S. Yamanaka, J. Alloys Compd. 469 (2009)50.

[69] T. J. Zhu, K. Xiao, C. Yu, J. J. Shen, S. H. Yang, A. J. Zhou, X. B. Zhao, J. He, J. Appl. Phys. 108(2010)044903.

[70] J. W. Simonson, D. Wu, W. J. Xie, T. M. Tritt, S. J. Poon, Phys. Rev. B, 83(2011)235211.

[71] M. Zhou, L. D. Chen, C. D. Feng, D. L. Wang, J. F. Li, J. Appl. Phys. 101 (2007)113714 .

[72] F. F. Wang, T. Fukuhara, K. Maezawa, S. Masubuchi, Jpn. J. Appl. Phys. 49 (2010)053002.

[73] X. G. Li, D. X. Huo, C. J. He, S. C. Zhao, Y. F. Lü, J. Inorg. Mater. 25(2010)573.

[74] C. Yu, T. J. Zhu, K. Xiao, J. J. Shen, S. H. Yang, X. B. Zhao, J. Electron. Mater. 39 (2010)2008.

[75] W. J. Xie, J. He, S. Zhu, X. L. Su, S. Y. Wang, T. Holgate, J. W. Graff, V. Ponnambalam, S. J. Poon, X. F. Tang, Q. J. Zhang, T. M. Tritt, Acta Mater. 58 (2010) 4705.

[76] R. Yaqub, P. Sahoo, J. P. A. Makongo, W. M. Nolting, N. Takas, P. F. P. Poudeu, K. L. Stokes, Mater. Res. Soc. Symp. Proc. 1267(2010)1.33

[77] P. Poudeu, 30th International Conference on Thermoelectrics, Traverse City, USA

[78] Y. Kimura, Y. Ueno, Y. Mishima, J. Electron. Mater. 38(2009)934.

[79] B. Balke, J. Barth, M. Schwall, G. H. Fecher, C. Felser, J. Electron. Mater. 40(2011) 702.

[80] G. A. Slack, V. G. Tsoukala, J. Appl. Phys. 76(1994)1665.

[81] X. Shi, W. Zhang, L. D. Chen, J. Yang, Phys. Rev. Lett. 95(2005)185503.

[82] G. J. Long, R. P. Hermann, F. Grandjean, E. E. Alp, W. Sturhahn, C. E. Johnson, D. E. Brown, O. Leupold, R. Ruffer, Phys. Rev. B, 71(2005)140320.

[83] E. R. Grannan, M. Randeria, and J. P. Sethna, Phys. Rev. B 41(1990) 7799.

[84] J. Yang, W. Zhang, S. Q. Bai, Z. Mei, L. D. Chen, Appl. Phys. Lett. 90(2007)192111.

[85] G. Rogl, A. Grytsiv, P. Rogl, E. Bauer, M. Zehetbauer, Intermetallics 19 (2011)546.

[86] L. Zhang, A. Grytsiv, M. Kerber, P. Rogl, E. Bauer, M. Zehetbauer, J. Alloys Compounds, 490(2010)19.

[87] M. Zebarjadi, K. Esfarjani, J. Yang, Z. F. Ren, G. Chen, Phys. Rev. B, 82(2010)195207.

[88] B. Duan, P. C. Zhai, L. S. Liu, Q. J. Zhang, J. Electrtronic Mater., 40(2011)932.

[89] X. L. Su, H. Li, Q. S. Guo, X. F. Tang, Q. J. Zhang, C. Uher, J. Electrtronic Mater., 40(2011)1286.

[90] X. L. Su, H. Li, G. Y. Wang, H. Chi, X. Y. Zhou, X. F. Tang, Q. J. Zhang, C. Uher, Chem. Mater. 23(2011)2948.

[91] Z. Xiong, X. Y. Huang, X. H. Chen, J. Ding, L. D. Chen, Scripta mater.62(2010)93.

[92] H. Kim, M. Kaviany, J. C. Thomas, A. Van der Ven, C. Uher, B. L. Huang, Phys. Rev. Lett. 105(2010)265901.

[93] H. Li, X. F. Tang, Q. J. Zhang, C. Uher, Appl. Phys. Lett. 94(2009)102114.

[94] Z. Xiong, X. H. Chen, X. Y. Huang, S. Q. Bai, L. D. Chen, Acta Mater. 58(2010)3995.

[95] C. Zhou, J. Sakamoto, D. Morelli, X. Y. Zhou, G. Y. Wang, C. Uher, J. Appl. Phys. 109(2011)063722.

[96] Q. M. Lu, J. X. Zhang, X. Zhang, 25th International Conference on Thermoelectrics, Vienna, AUSTRIA, 2006, pp.148-150.

[97] Y. Z. Pei, A. LaLonde, S. Iwanaga, G. J. Snyder, Energy Environ. Sci. 4(2011)2085.

[98] A. LaLonde, Y. Z. Pei, G. J. Snyder, Energy Environ. Sci. 4(2011)2090.

[99] J. Q. He, J. R. Sootsman, S. N. Girard, J. C. Zheng, J. G. Wen, Y. M. Zhu, M. G. Kanatzidis, V. P. Dravid, J. Am. Chem. Soc 132(2010)8669.

[100] J. R. Sootsman, H. J. Kong, C. Uher, J. J. D'Angelo, C. I. Wu, T. P. Hogan, T. Caillat, M. G. Kanatzidis, Angew. Chem. Int. ed. 47(2008)8618.

[101] P. F. P. Poudeu, J. J. D'Angel, A. D. Downey, J. L. Short, T. P. Hogan. M. G. Kanatzidis, Angew. Chem. Int. ed. 45(2006)3835.

[102] J. Androulakis, C. H. Lin, H.J. Kong, C. Uher, C. I. Wu, T. Hogan, B. A. Cook, T. Caillat, K. M. Paraskevopoulos, M. G. Kanatzidis, J. Am. Chem. Soc. 129(2007)9780.

[103] K. Ahn, M. K. Han, J. Q. He, J. Androulakis, S. Ballikaya, C. Uher, V. P. Dravid, M. G. Kanatzidis, J. Am. Chem. Soc. 132(2010)5227.

[104] Y. Z. Pei, J. Lensch-Falk, E. S. Toberer, D. L. Medlin, G. J. Snyder, Adv. Funct. Mater. 21(2011)241.

[105] S. Johnsen, J. Q. He, J. Androulakis, V. P. Dravid, I. Todorov, D. Y. Chung, M. G. Kanatzidis, J. Am. Chem. Soc. 133(2011)3460.

[106] D. T. Morelli, V. Jovovic, J. P. Heremans, Phys. Rev. Lett. 101(2008)035901.

[107] J. J. Xu, H. Li, B. L. Du, X. F. Tang, Q. J. Zhang, C. Uher, J Mater. Chem. 20(2010)6138.

[108] H. Wang, J. F. Li, M. M. Zou, T. Sui, Appl. Phys. Lett. 93(2008)202106.

[109] L. D. Zhao, B. P. Zhang, J. F. Li, W. S. Liu, Solid State Sci. 10(2008)651.

[110] X. Yan, B. Poudel, Y. Ma, W. S. Liu, G. Joshi, H. Wang, Y. C. Lan, D. Z. Wang, G. Chen, Z. F. Ren, Nano Lett.10(2010)3373.

[111] S. Miura, Y. Sato, K. Fukuda, K. Nishimura, K. Ikeda. Mater. Sci. Eng. A 277(2000) 244

[112] Y. C. Lan, D. Z. Wang, G. Chen, Z. F. Ren, Appl. Phys. Lett. 92(2008)101910.

[113] M. K. Han, K. Ahn, H. J. Kim, J. S. Rhyeec, S. J. Kim. J. Mater. Chem. 21(2011) 11365.

[114] D. K. Ko, Y. J. Kang, C. B. Murray, Nano Lett., 11(2011)2841.

[115] D. W. Liu, J. F. Li, C. Chen, B. P. Zhang, J. Electronic Mater. 40(2011)992.

[116] X. H. Ji, J. He, Z. Su, N. Gothard, Tritt T. M., J. Appl. Phys. 104(2008)034907.

[117] Q. Zhang, Q. Y. Zhang, S. Chen, W. S. Liu, K. Lukas, X. Yan, H. Z. Wang, D. Z. Wang, C. Opeil, G. Chen, Z. F. Ren, Nano Energy 1(2012)183-189.

[118] M. Zebarjadi, G. Joshi, G. H. Zhu, B. Yu, A. Minnich, Y. C. Lan, X. W. Wang, M. Dresselhaus, Z. F. Ren. G. Chen, Nano Lett. 11(2011)2225.

[119] R. Venkatasubramanian, E. Siivola, T. Colpitts, B. O'Quinn, Nature 413(2001)597.

[120] J. Y. Tang, H. T. Wang, D. H. Lee, M. Fardy, Z. Y. Huo, T. P. Russell, P. D. Yang, Nano Lett.10(2010)4279.

[121] Y. P. He, D. Donadio, J. H. Lee, J. C. Grossman, G. Galli, ACS Nano, 3(2011)1839.

Caption of Figures

Figure 1. Power generation efficiency φ_{te} of single-leg state-of-the-art nanocomposites as a function of temperature difference T_h with an assumption of T_c = 300 K. $Sb_xBi_{2-x}Te_3$ [5], $Cu_xBi_2Te_{2.7}Se_{0.3}$ [6], $AgPb_{m+2}SbTe_m$ [7], Zn_4Sb_3 **Error! Reference source not found.**, $In_4Se_{3-x}Cl_x$ [8], $Tl_xPb_{1-x}Te$ **Error! Reference source not found.**, $DD_xFe_3CoSb_{12}$ [10], $Sr_xPb_xTe_3$ [12], Na_xPbSe [13], $CoSb_{3-x-y}Te_xSn_y$ [14], Al_xPbSe [15], p-half Heusler [16], n-half-Heusler [17], $Ba_xLa_yYb_zCo_4Sb_{12}$ [18], n-type SiGe [19], and p-type SiGe [20]. DD (Didymium, 4.76 mass% Pr and 95.24 mass% Nd) is nature mixture of rare earth elements.

Figure 2. (a) Ideal $F\bar{4}3m$ structure of half-Heusler ABX, (b) the reported elements for the A, B and X sublattices shown in a partial periodical table.

Figure 3. Typical TEM images for half-Heusler nanocomposite made from ball milling plus hot pressing (BM-HP) method. (a) low magnification TEM image of nanostructured $Hf_{0.5}Zr_{0.5}CoSb_{0.8}Sn_{0.2}$ [16], (b) low magnification TEM image of nanostructured $Hf_{0.75}Zr_{0.25}NiSn_{0.99}Sb_{0.01}$ [17], (c) nano inclusion embedded in $Hf_{0.5}Zr_{0.5}CoSb_{0.8}Sn_{0.2}$ matrix [16], (d) distorted lattice in nanostructured $Hf_{0.75}Zr_{0.25}NiSn_{0.99}Sb_{0.01}$ [17]. The insets in (a) and (d) indicate the grains have good crystalline structures.

Figure 4. Temperature-dependent Seebeck coefficient (a, b), thermal conductivity (c, d), and ZT value (e, f) of p-type $Hf_{0.5}Zr_{0.5}CoSb_{0.8}Sn_{0.2}$[16], and n-type $Hf_{0.75}Zr_{0.25}NiSn_{0.99}Sb_{0.01}$ [17] nanocomposites.

Figure 5. Ideal $Im\bar{3}$ structure of skutterudite MX_3 with M site located at 8c (0.25, 0.25, 0.25) site and X locates at 24g (0, v, w) site. An intrinsic nano-cage located at 2a (0, 0, 0) site.

Figure 6, (a) Room temperature (300 K) and (b) high-temperature (850 K) lattice thermal conductivity of filled skutterudites as a function of total filling fraction for single-,

double-, and triple- filled skutterudites. The solid lines are guidance to the eyes. Estimated high power factor region (between the red vertical lines) are also shown to demonstrate how to simultaneously maximize power factors and minimize lattice thermal conductivity [18].

Figure 7. Raman shift of $CoSb_{2.86}M_{0.02}Te_{0.12}$ (M=Sb, Si, Ge, Sn, Pb) [14].

Figure 8. Temperature-dependent ZT value of (a) p-type PbTe with varying Sodium [97] and (b) n-type PbTe with varying Iodine [98].

Figure 9. Reduced lattice thermal conductivity of PbTe-based nanocomposite with various nanoinclusions, including Bi [100], Pb [100], Sb [100], SrTe [12], $AgSbTe_2$ [7], $NaSbTe_2$ [101], PbS [102], CdTe [103], and Ag_2Te [104].

Figure 10. TEM images of Cu-doped Bi_2Te_3-based nanocomposite: (a) and (b) nano stripes due to local stress when Cu gets into the interstitial site between Van der Waals bound two Te layers [6]. (c) and (d) nano particles due the precipitation of Cu from the Bi_2Te_3 matrix [113].

Figure 11. Comparison of various nanostructures between random nanocomposites (a-e) and ordered nanocomposite (f-j) from doping atom, nanoinclusions, grain boundaries, grain shape, to void morphology. The idea of ordered nanocomposite is a new proposal concept with various well-organized nanostructures to reconstruct the electron transport channel, which is in contrast to most current thermoelectric nanocomposite with un-tailored nanostructures.

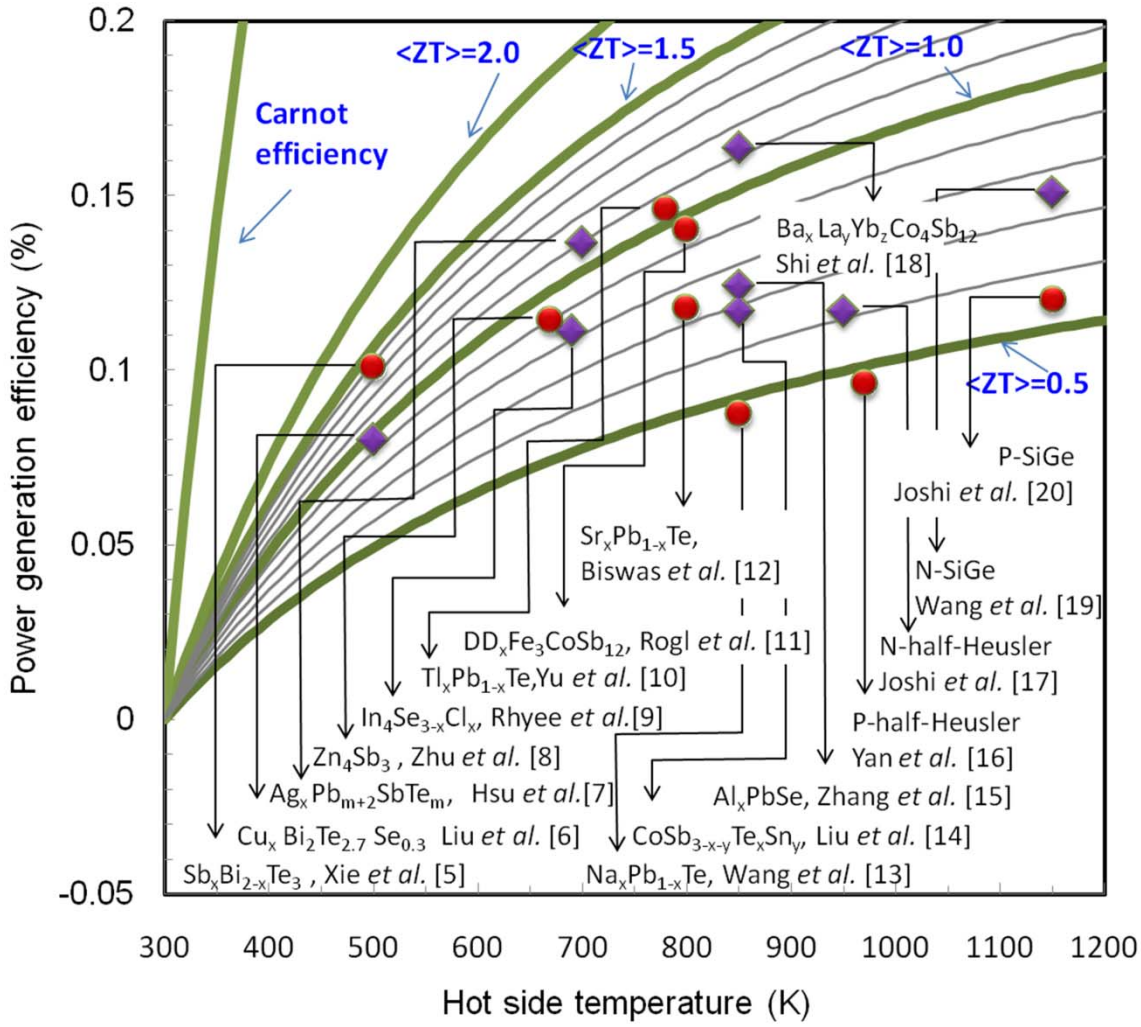

Figure 1, W. S. Liu *et al.*

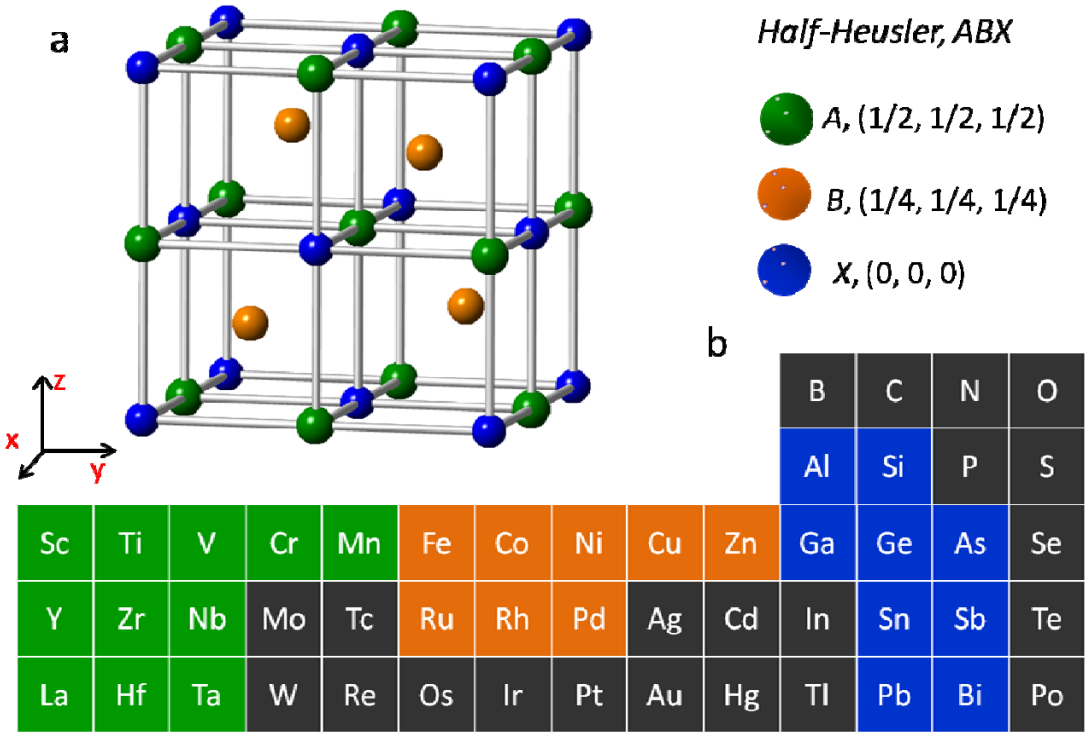

Figure 2, W. S. Liu *et al.*

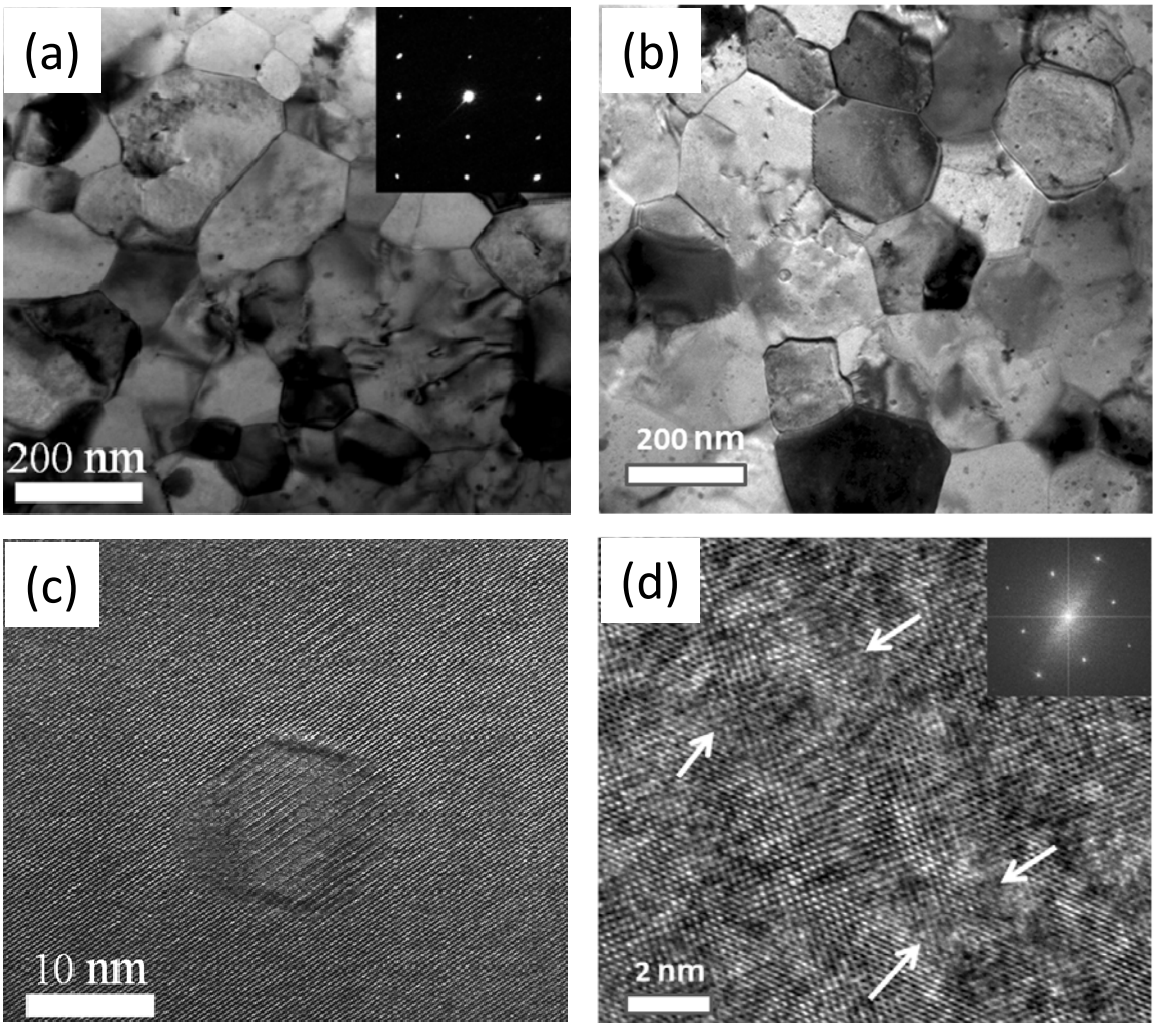

Figure 3, W. S. Liu *et al.*

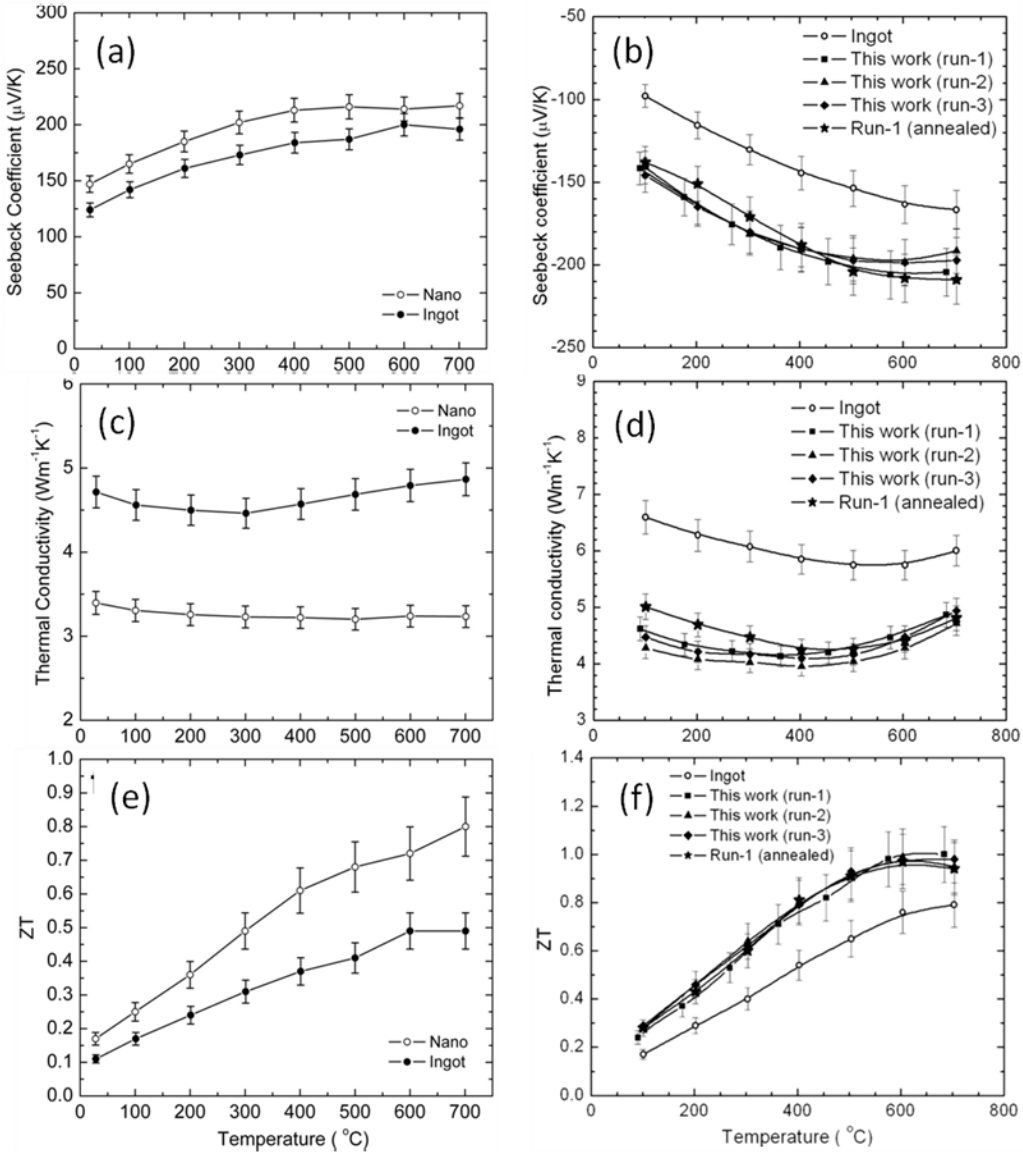

Figure 4, W. S. Liu *et al.*

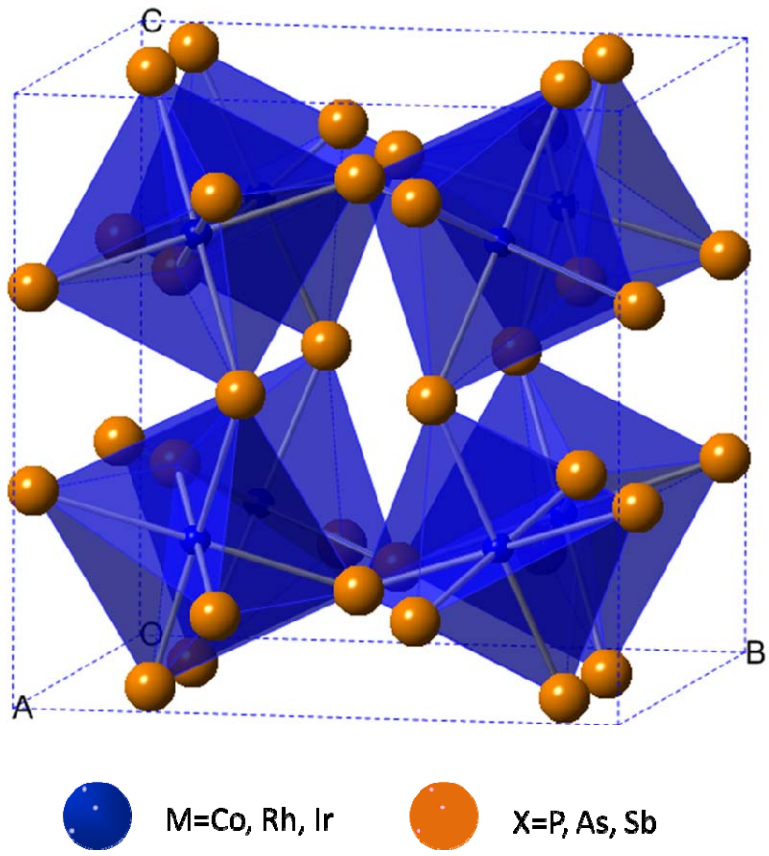

Figure 5, W. S. Liu *et al.*

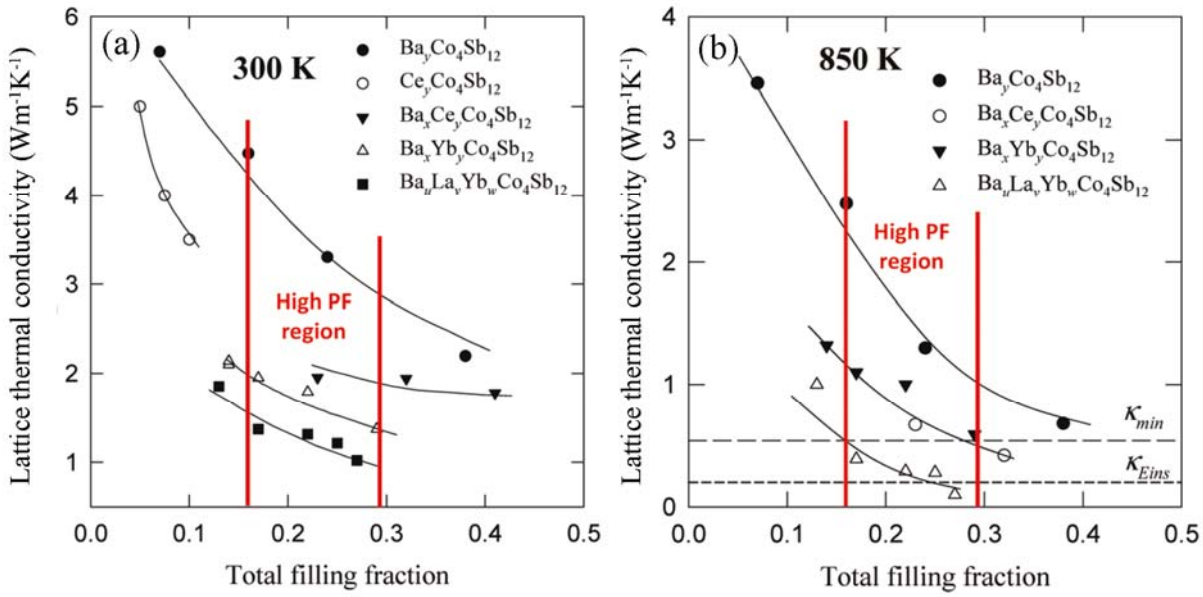

Figure 6, W. S. Liu *et al.*

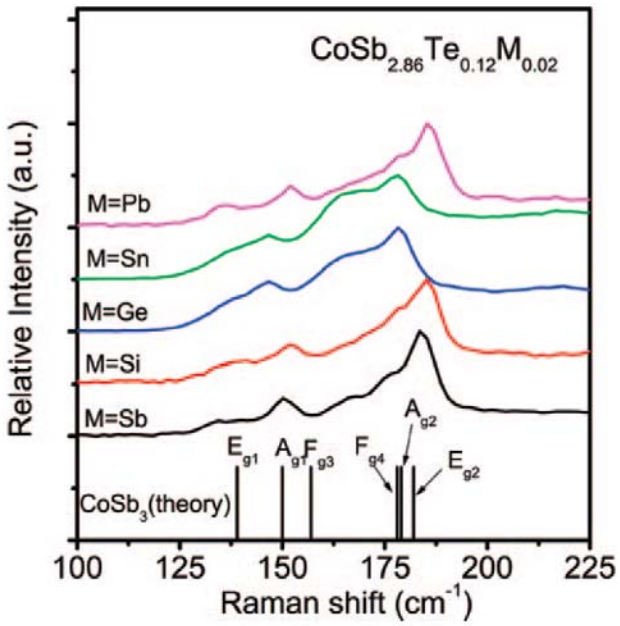

Figure 7. W. S. Liu *et al.*

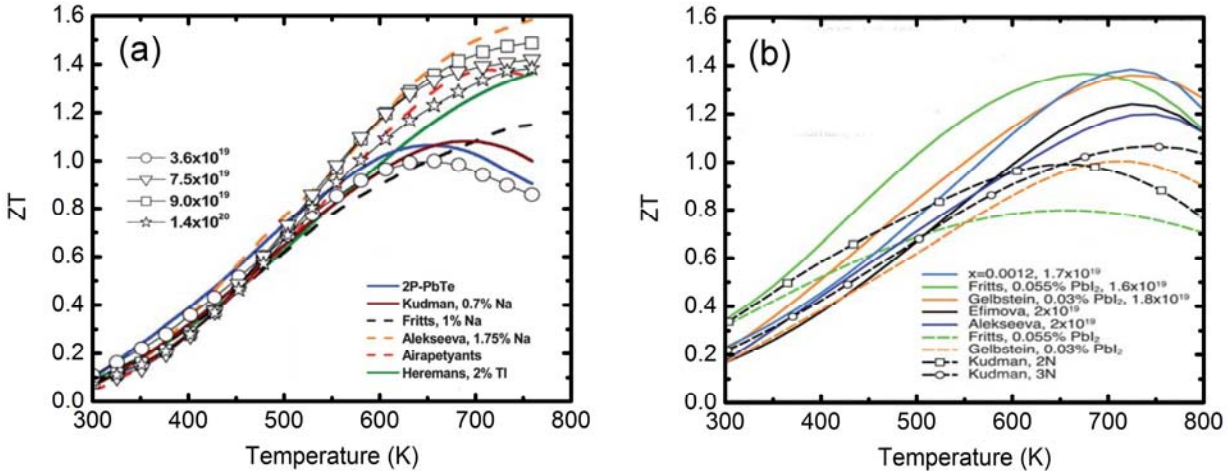

Figure 8. W. S. Liu *et al.*

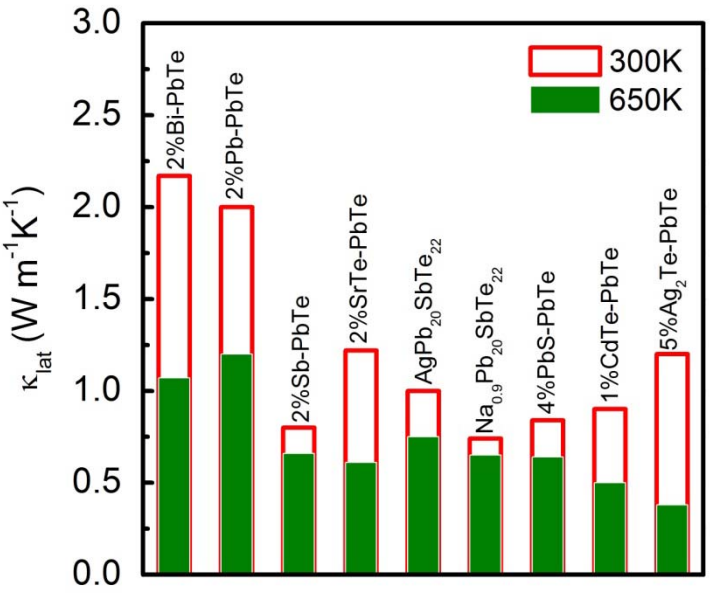

Figure 9. W. S. Liu et. al.

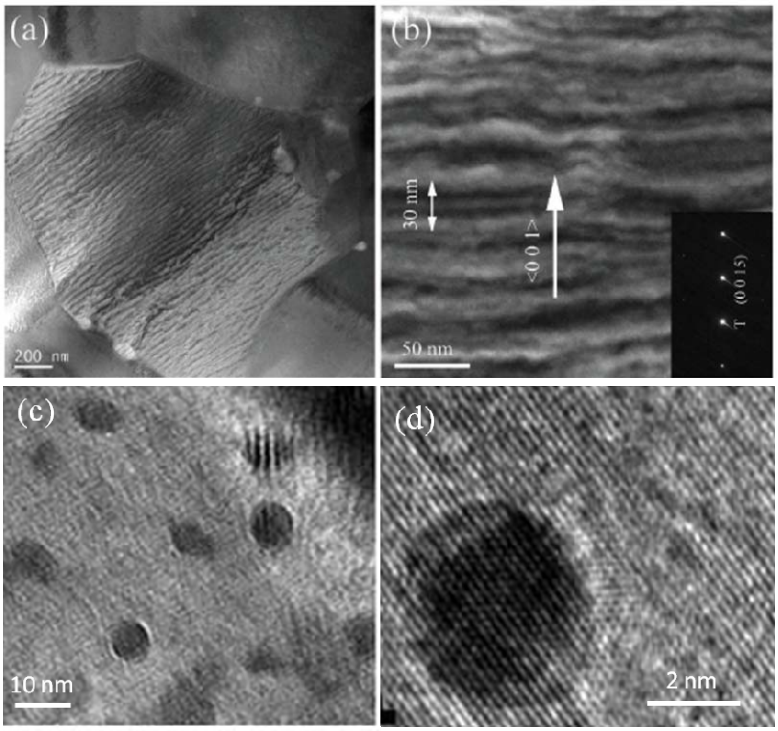

Figure 10. W. S. Liu et. al.

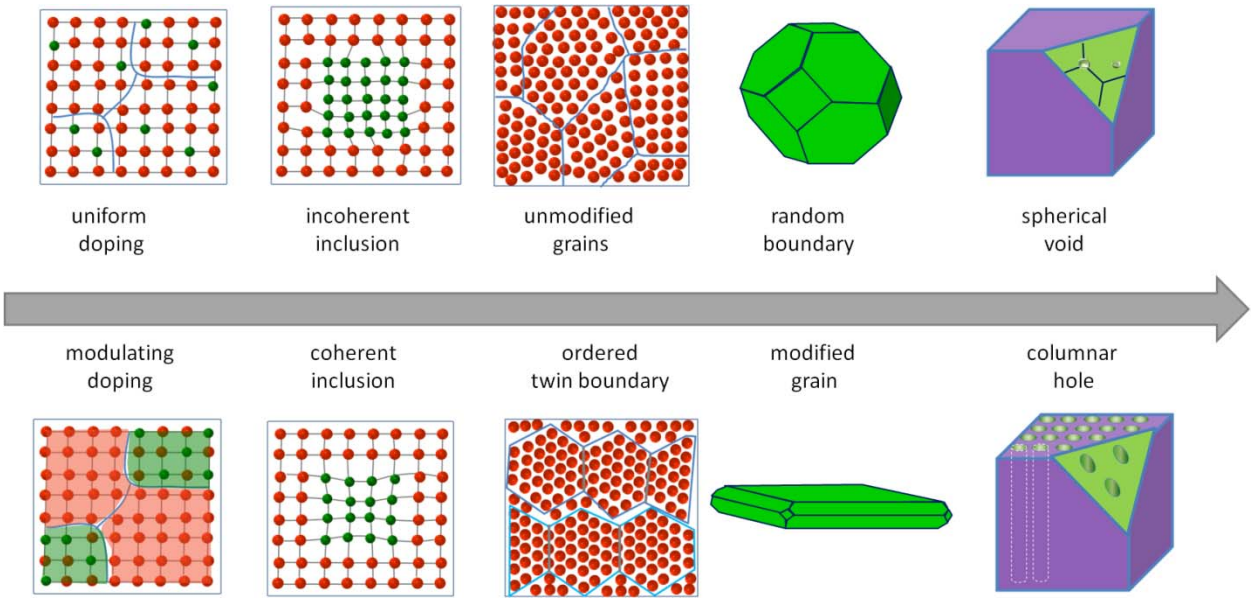

Figure 11. W. S. Liu et. al.